Coherent population trapping in Raman-pulse atom interferometry

Coherent population trapping in Raman-pulse atom interferometry

David L. Butts,[1,2] Joseph M. Kinast,[2] Krish Kotru,[1,2] Antonije M. Radojevic,[2] Brian P. Timmons,[2] and Richard E. Stoner[2]
[1]*Department of Aeronautics & Astronautics, Massachusetts Institute of Technology, Cambridge, Massachusetts 02139, USA*
[2]*C.S. Draper Laboratory, Incorporated, Cambridge, Massachusetts 02139, USA*
(Received 9 June 2011; published 10 October 2011)

Raman pulse atom interferometry is an important modality for precision measurements of inertial forces and tests of fundamental physics. Typical Raman atom optics use two coherent laser fields applied at gigahertz-scale detunings from optical resonance, so that spontaneous emission produces a minor or negligible source of decoherence. An additional consequence of spontaneous emission is coherent population trapping (CPT). We show that CPT produces coherences and population differences which induce systematic effects in Raman pulse atom interferometers. We do not believe that CPT has been previously identified as an error mechanism in Raman pulse atom interferometry. We present an experimental characterization of CPT coherences and population differences induced in laser-cooled cesium atoms by application of Raman pulses at detunings near 1 GHz, commensurate with detunings used in several precision measurement experiments. We are not aware of previous demonstrations of CPT-induced population difference. We argue that CPT effects could induce phase shifts of several milliradians in magnitude for typical experimental parameters and stipulate that these errors can be suppressed by propagation direction reversal in Raman interferometer-based precision measurements.

DOI: 10.1103/PhysRevA.84.043613 PACS number(s): 03.75.Dg, 42.81.Pa

I. INTRODUCTION

Atom interferometry provides sensitive measurements of inertial forces for inertial navigation and geophysical applications, as well as tests of fundamental physics. At present, state-of-the-art atom interferometric inertial sensors utilize light pulses [1–4] rather than mechanical gratings for coherent manipulation of matter waves. Light-pulse atom beam splitters offer several advantages, including high transmission efficiency and suitability for increasing interrogation time and sensitivity in atomic fountain configurations. Most implementations of light-pulse atom interferometers use stimulated Raman transitions as the atom beam splitter and mirror. While other light-pulse beam splitters, such as multiphoton Bragg pulses [5] and Bloch oscillations [4,6], can achieve larger momentum transfer and potentially offer higher interferometer sensitivity, Raman pulse beam splitters are relatively simple to implement and place less stringent requirements on atom temperature and laser power.

Both existing and future tests of fundamental physics with atom interferometry and high-precision inertial sensing technology demand critical investigations of light-based systematic error sources (e.g., [7]). Analyses of stimulated Raman transitions in the open literature commonly neglect the effects of spontaneous emission, or treat it solely as a source of decoherence (e.g., [8]). An additional consequence of spontaneous emission is coherent population trapping (CPT), or the transfer of atomic population to a decoupled (dark) superposition state. CPT has been extensively analyzed and observed experimentally in three-level (Λ) atomic systems with Raman resonances excited by bichromatic laser fields [9–11]. Since the discovery of the effect, it has been exploited for precision measurement applications including chip-scale atomic clocks [12] and atomic magnetometry [13], in which narrow rf resonances are achieved in steady-state laser operation. However, possible residual non-steady-state CPT effects in atom interferometry with stimulated Raman transitions have not been discussed in the literature. This work addresses the impact of transient CPT effects on Raman pulse atom interferometry. We argue that interferometer phase shifts of multiple milliradians in amplitude have likely been produced in some Raman pulse interferometry applications, although we do not think the accuracy of these measurements was significantly affected.

We begin by summarizing an elementary density matrix theory for calculating Raman pulse output state populations and coherences that, by including spontaneous emission, predicts CPT effects. We then present measurements of dark-state coherences and population differences induced in cold cesium atoms by velocity-sensitive and velocity-insensitive Raman pulses. Finally, we make a simple argument that dark-state coherences induced by a Raman pulse beam splitter shift the phase of a three-pulse atom interferometer and propose that propagation direction reversal [14] should suppress the phase error.

II. THEORY

Stimulated Raman transitions in atom interferometry have previously been described using Schrödinger formalism [8,15], in which spontaneous emission effects were not considered. Raman pulses used as atomic beam splitters are typically detuned from optical resonance by $\sim$1 GHz or more, so that spontaneous emission causes minimal decoherence. However, we show that the presence of spontaneous emission can be expected to result in creation of dark-state coherences, even in the large detuning regime of relevance to Raman pulse atom interferometry.

In this section we summarize a three-state density matrix theory for Raman pulse physics that motivates and qualitatively describes our experimental results. This model only approximately describes a real atom, but we argue that it captures the essential physics and permits an analytic solution. The theory includes spontaneous emission in a three-state (Λ) atom, as depicted in Fig. 1. We argue that for relatively large laser detunings $|\Delta| \geqslant 1$ GHz, the time derivatives of

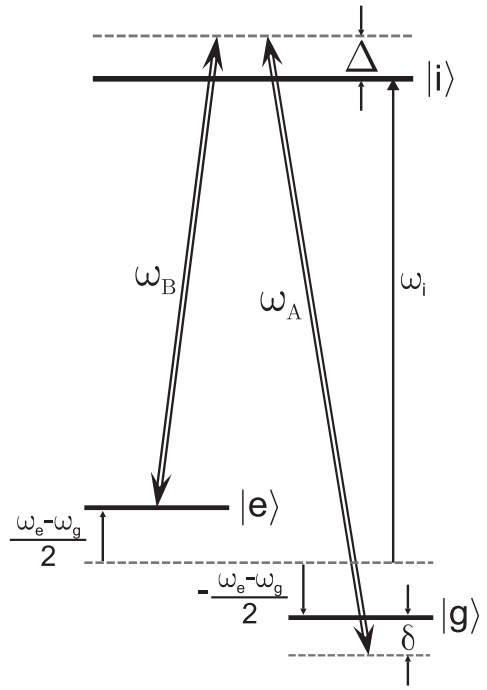

FIG. 1. Diagram of the three-level (Λ) atom and laser fields considered in Sec. II.

the ground-excited state coherences can be neglected, leading to a simple analytic solution. Prior to exhibiting solutions, the problem will be recast in terms of a pseudospin vector polarization on a Bloch sphere. It is shown that in addition to "torquing" an initial polarization state in a fashion exactly analogous to rf spin resonance in nuclear magnetic resonance, the Raman pulse will induce a dark-state polarization.

Consider an atom with two closely spaced ground states, $|g\rangle$ and $|e\rangle$, and a single excited state $|\mathrm{i}\rangle$ (Fig. 1). Ground state $|g\rangle$ ($|e\rangle$) is coupled by electric field $\vec{E}_A$ ($\vec{E}_B$) to $|\mathrm{i}\rangle$. The analysis is placed in a reference frame comoving with the atom in $|g\rangle$, and therefore the frequencies of the applied fields depend on the motional state of the atom [15]. We define the fields $\vec{E}_A$, $\vec{E}_B$ as

$$\vec{E}_A = \hat{e}_A \varepsilon_A \cos\left[\phi_A(t) + \phi_A^0\right], \tag{1}$$

$$\vec{E}_B = \hat{e}_B \varepsilon_B \cos\left[\phi_B(t) + \phi_B^0\right], \tag{2}$$

with $\phi_A(t) = \int_0^t [\omega_A(t') - \vec{k}_A \cdot \hat{e}_z \dot{z}(t)]dt'$, $\phi_B(t) = \int_0^t [\omega_B(t') - \vec{k}_B \cdot \hbar\vec{k}_{\mathrm{eff}}/m - \vec{k}_B \cdot \hat{e}_z \dot{z}(t)]dt'$, polarization vectors $\hat{e}_j$, amplitudes ε_j, time-dependent frequencies ω_j, wave vectors $\vec{k}_j$, two-photon effective wave vector $\vec{k}_{\mathrm{eff}} = \vec{k}_A - \vec{k}_B$, and phases ϕ_j^0 for field $\vec{E}_j$. The two wave vectors are assumed to be either parallel or antiparallel to each other, with both aligned along $\hat{e}_z$. The derivation accounts for both copropagating (velocity insensitive) and counterpropagating (velocity sensitive) cases. The two-photon recoil velocity $\hbar\vec{k}_{\mathrm{eff}}/m$ is included in the velocity of an atom in state $|e\rangle$, which couples to $\vec{E}_B$; the Doppler shift of $\vec{E}_B$ thus contains a recoil contribution. The optical phases are defined with time-dependent frequencies to address the interrogation of atoms accelerating relative to the Raman beams, which is applicable to the gravimeter configuration in our experiments.

The energy origin for the atom is chosen to be the midpoint between the ground-state energies $\hbar\omega_e$ and $\hbar\omega_g$, as shown by Fig. 1. The laser detuning Δ from the optical resonances, as well as the Raman detuning δ between the laser frequency difference and the ground-state energy-level splitting, are indicated in Fig. 1. These detunings are defined here as

$$\delta(t) \equiv [\omega_A(t) - \omega_B(t)] - \left[(\omega_e - \omega_g) + \frac{\hbar\vec{k}_{\mathrm{eff}}^2}{2m} - \frac{\hbar}{2m}\left(k_A^2 - k_B^2\right) + \vec{k}_{\mathrm{eff}} \cdot \dot{z}(t)\hat{e}_z\right], \tag{3}$$

$$\Delta \equiv \frac{\omega_A(t) + \omega_B(t)}{2} - \left[\omega_{\mathrm{i}} - \frac{1}{2}\left(\frac{\hbar\vec{k}_{\mathrm{eff}}^2}{2m} - \frac{\hbar}{2m}\left(k_A^2 - k_B^2\right) - \left(\vec{k}_A + \vec{k}_B\right) \cdot \dot{z}(t)\hat{e}_z\right)\right]. \tag{4}$$

The Hamiltonian, including both internal (diagonal elements) and field interaction (off-diagonal elements) dynamics, is

$$\hat{H} = \frac{\hbar}{2}\begin{bmatrix} \omega_e - \omega_g & \Omega_B e^{i\phi_B(t)} & 0 \\ \Omega_B^* e^{-i\phi_B(t)} & 2\omega_{\mathrm{i}} & \Omega_A^* e^{-i\phi_A(t)} \\ 0 & \Omega_A e^{i\phi_A(t)} & -(\omega_e - \omega_g) \end{bmatrix}, \tag{5}$$

where $\Omega_j = |\Omega_j| e^{i\phi_j^0}$ is the complex Rabi frequency associated with the coupling for field $\vec{E}_j$. The time dependence of the Hamiltonian can be factored out using a unitary transformation defined by

$$\hat{U}_{\mathrm{int}} \equiv \exp\{-\hat{P}_e \frac{i}{2}[(\omega_e - \omega_g) + \delta(t)]\} + \exp\{\hat{P}_g \frac{i}{2}[(\omega_e - \omega_g) + \delta(t)]\} + \exp[-\hat{P}_{\mathrm{i}} i(\Delta + \omega_{\mathrm{i}})], \tag{6}$$

where $\hat{P}_e$, $\hat{P}_{\mathrm{i}}$, $\hat{P}_g$ are the Hilbert space projection operators onto states $|e\rangle$, $|\mathrm{i}\rangle$, and $|g\rangle$, respectively. In terms of Eq. (5), the Hamiltonian can be written as

$$\hat{H} = \hbar\hat{U}_{\mathrm{int}} \begin{bmatrix} \frac{1}{2}(\omega_e - \omega_g) & \frac{1}{2}\Omega_B & 0 \\ \frac{1}{2}\Omega_B^* & \omega_{\mathrm{i}} - \frac{1}{2}(\omega_e + \omega_g) & \frac{1}{2}\Omega_A^* \\ 0 & \frac{1}{2}\Omega_A & -\frac{1}{2}(\omega_e - \omega_g) \end{bmatrix} \hat{U}_{\mathrm{int}}^\dagger. \tag{7}$$

The density matrix ρ for the three-level system is

$$\rho = \begin{bmatrix} \rho_{ee} & \rho_{ei} & \rho_{eg} \\ \rho_{ie} & \rho_{ii} & \rho_{ig} \\ \rho_{ge} & \rho_{gi} & \rho_{gg} \end{bmatrix}. \tag{8}$$

The time rate of change of the density matrix due to spontaneous emission is

$$\dot{\rho}_{SE} = \begin{bmatrix} \frac{\Gamma}{2}\rho_{ii} & -\frac{\Gamma}{2}\rho_{ei} & 0 \\ -\frac{\Gamma}{2}\rho_{ie} & -\Gamma\rho_{ii} & -\frac{\Gamma}{2}\rho_{ig} \\ 0 & -\frac{\Gamma}{2}\rho_{gi} & \frac{\Gamma}{2}\rho_{ii} \end{bmatrix}, \tag{9}$$

where Γ is the average rate of spontaneous decay from the excited state [16]. For simplicity, we have assumed a closed system in which excited-state decay is restricted to the two ground states with equal branching ratios, and we neglect any decay of the ground-state coherences. The equation of motion for the density matrix is

$$\frac{d\rho}{dt} = \frac{1}{i\hbar}[\hat{H},\rho] + \dot{\rho}_{SE}. \tag{10}$$

We now transform this equation to the interaction picture using $\hat{U}_{\rm int}$ and by representing the interaction picture density matrix $R_{\rm int}$ as

$$R_{\rm int} \equiv \begin{bmatrix} \rho_{ee} & r_{ei} & r_{eg} \\ r_{ie} & \rho_{ii} & r_{ig} \\ r_{ge} & r_{gi} & \rho_{gg} \end{bmatrix} = \hat{U}_{\rm int}^{\dagger}\rho\hat{U}_{\rm int}. \tag{11}$$

The equations governing the ground-excited state coherences (r_{ei} and r_{gi}) can be simplified first by noting that for typical experimental conditions, $|\delta(t)| \ll |\Delta|$. Adiabatic elimination, wherein a large rate is taken to dominate time evolution, permits an approximate solution for the ground-excited state coherences:

$$\frac{d}{dt}R_{\rm int} \cong \frac{d}{dt}\begin{bmatrix} \rho_{ee} & 0 & r_{eg} \\ 0 & \rho_{ii} & 0 \\ r_{ge} & 0 & \rho_{gg} \end{bmatrix}. \tag{12}$$

It can then be shown, from the approximate equation of motion for $R_{\rm int}$, that

$$r_{ei} \cong \frac{\Omega_A r_{eg} - \Omega_B(\rho_{ii} - \rho_{ee})}{2\Delta - i\Gamma}, \tag{13}$$

$$r_{ig} \cong \frac{\Omega_A^*(\rho_{gg} - \rho_{ii}) + \Omega_B^* r_{eg}}{2\Delta + i\Gamma}. \tag{14}$$

Substituting these relations back into the equation of motion, and making the additional assumption that the excited-state population $\rho_{ii} \ll 1$, reduces the original equation of motion to an equation for populations ρ_{ee}, ρ_{gg} and coherence r_{eg}. At this point we define components for a pseudospin $\vec{P}(t)$ on a Bloch sphere

$$P_j(t) = \mathrm{Tr}\left(\begin{bmatrix} \rho_{ee} & r_{eg} \\ r_{ge} & \rho_{gg} \end{bmatrix} \cdot \sigma_j\right), \quad j = x,y,z, \tag{15}$$

where $\{\sigma_j\}$ are the Pauli spin matrices. Thus

$$\vec{P}(t) = \begin{bmatrix} P_x(t) \\ P_y(t) \\ P_z(t) \end{bmatrix} = \begin{bmatrix} 2\mathrm{Re}[r_{\rm eg}] \\ -2\mathrm{Im}[r_{\rm eg}] \\ \rho_{ee} - \rho_{gg} \end{bmatrix}. \tag{16}$$

A similar transformation was used in [17], though spontaneous emission was not considered.

We now state the results of a lengthy but elementary analysis in which we substitute the pseudospin components from Eq. (16) into the equation of motion for $R_{\rm int}$, apply adiabatic elimination as per Eq. (12), and assume that $\rho_{ii} \ll 1$. The approximate vector equation of motion for $\vec{P}(t)$ is

$$\frac{d}{dt}[\vec{P}(t) - \vec{P}_{\rm dark}] + [\vec{P}(t) - \vec{P}_{\rm dark}] \times \vec{\Omega} + \Gamma_{\rm loss}[\vec{P}(t) - \vec{P}_{\rm dark}] \cong -\hat{e}_z\Gamma_{\rm source}, \tag{17}$$

where

$$\begin{aligned} \vec{P}_{\rm dark} &\equiv -\frac{\vec{\Omega}}{\Omega_{e,AC} + \Omega_{g,AC}}, \\ \Gamma_{\rm source} &= \frac{\Gamma\delta}{2\Delta}, \\ \Gamma_{\rm loss} &= \frac{\Gamma}{2\Delta}(\Omega_{e,AC} + \Omega_{g,AC}), \\ \Omega_{j,AC} &= \frac{|\Omega_j|^2}{4\Delta}, \\ \delta_{AC} &= \Omega_{e,AC} - \Omega_{g,AC}, \\ \vec{\Omega} &= \Omega[\cos\theta\hat{z} + \sin\theta(\cos\phi\hat{x} + \sin\phi\hat{y})], \\ \Omega &= \sqrt{|\Omega_{\rm eff}|^2 + (\delta_{\rm AC} - \delta)^2}, \\ \cos\theta &= \frac{\delta_{AC} - \delta}{\Omega}, \quad \sin\theta = \frac{|\Omega_{\rm eff}|}{\Omega}, \\ \phi &= \phi_A^0 - \phi_B^0, \\ \Omega_{\rm eff} &= \frac{\Omega_A\Omega_B^*}{2\Delta} = \frac{|\Omega_A||\Omega_B|e^{i\phi}}{2\Delta}. \end{aligned} \tag{18}$$

Equation (17) is analogous to the dynamics for a classical magnetization subjected to a magnetic field torque and decoherence, with a source of longitudinal magnetization. This equation can be solved with the use of a concise notation. Given a fixed vector $\vec{\alpha} = \alpha\hat{\alpha}$, we define an exponentiated cross-product operator acting on an arbitrary vector $\vec{V}$ as

$$\begin{aligned} \exp[\alpha(\hat{\alpha}\times)]\vec{V} &= [\cos\alpha(\mathbf{1}\cdot) + \sin\alpha(\hat{\alpha}\times) + (1-\cos\alpha)\hat{\alpha}(\hat{\alpha}\cdot)]\vec{V} \\ &= \cos\alpha\,\vec{V} + \sin\alpha(\hat{\alpha}\times\vec{V}) \\ &\quad + (1-\cos\alpha)\hat{\alpha}(\hat{\alpha}\cdot\vec{V}). \end{aligned} \tag{19}$$

This exponentiated cross-product operator acts to rotate $\vec{V}$ about $\hat{\alpha}$ in the right-hand sense by an angle α. The expression in Eq. (19) can be obtained by Taylor expansion and the application of cross-product rules. It is simple to show that the derivative of this operator is

$$\frac{d}{d\alpha}\exp[\alpha(\hat{\alpha}\times)] = \hat{\alpha}\times\exp[\alpha(\hat{\alpha}\times)]. \tag{20}$$

With this rotation operator definition, it can be shown that the solution to Eq. (17) for the time-dependent pseudospin is

$$\begin{aligned} \vec{P}(t) &= \exp\{[\Omega(\hat{\Omega}\times) - \Gamma_{\rm loss}\cdot\mathbf{1}]t\}\cdot\vec{P}(0) \\ &\quad + \{\exp[(\Omega(\hat{\Omega}\times) - \Gamma_{\rm loss}\cdot\mathbf{1})t] - \mathbf{1}\} \\ &\quad \times\{\vec{P}_{\rm dark} - [-\Omega(\hat{\Omega}\times) + \Gamma_{\rm loss}\cdot\mathbf{1}]^{-1}\cdot(\Gamma_{\rm source}\hat{e}_z)\}. \end{aligned} \tag{21}$$

We note that $\Gamma_{\rm loss}$ cannot vanish on physical grounds, so that the inverse in the final term of Eq. (21) always exists. This solution represents the pseudospin polarization in the rotating frame. As expected, the action of the Raman pulse on the initial polarization is to rotate it about the Raman effective drive field, $\vec{\Omega}$. There is also a slow loss of coherence due to spontaneous emission. However, in addition to the torquing action on the initial polarization, another polarization is induced, with an asymptotic value of

$$\vec{P}(t\rightarrow\infty) = -\vec{P}_{\rm dark} + [-\Omega(\hat{\Omega}\times) + \Gamma_{\rm loss}\cdot\mathbf{1}]^{-1}\cdot(\Gamma_{\rm source}\hat{e}_z). \tag{22}$$

On resonance, this expression simplifies to $\vec{P}(t\rightarrow\infty) = -\vec{P}_{\rm dark}$. Recalling the definition for $\vec{P}_{\rm dark}$, we note that for negative laser detunings ($\Delta < 0$) the asymptotic polarization is induced parallel to the effective drive field $\vec{\Omega}$. The dark polarization is aptly named since $\hat{\Omega}\times\vec{P}_{\rm dark} = 0$, i.e., the optical fields do not couple to it.

This theory can only be expected to provide a qualitative description of Raman pulse physics in the ground-state hyperfine manifold of a real alkali-metal atom, given the simple Λ structure considered here. In this closed system, spontaneous decay returns atoms to one of the coupled ground states. In an alkali atom, spontaneous emission can remove an atom from further interaction via decay to an uncoupled ground state. We have also neglected the effect of multiple excited states. Selection rules permit two excited-state hyperfine sublevels to act as intermediaries in Raman transitions. The coupling of the ground states to the two intermediaries is comparable for the range of detunings considered here ($\Gamma \ll \Delta \ll \omega_e - \omega_g$). Therefore we expect substantial deviations between the present theory and experiment. Since no ground-state superposition will be "dark" with respect to two possible intermediary excited states, continued coupling to the field will result in decreasing magnitudes of induced polarization at long pulse lengths. The theory, by contrast, predicts large asymptotic polarizations, of magnitude approaching unity for excitation close to the Raman resonance.

We note that for nonresonant pulses, the theory predicts that a population difference between the ground states is induced in addition to coherence between the ground states. In addition, the time evolution of the polarization, when scaled by the pulse area Ωt, is predicted to be independent of the effective Rabi frequency. The approximations employed in the theory would not appear to compromise this prediction. While a more accurate numerical simulation of a real atom is not included in this work, such a study is feasible and constitutes an interesting step for future work. In the next section we see that the qualitative predictions of the theory are experimentally realized, supporting our assertion that the observed effects are induced by CPT.

III. EXPERIMENT

In this section we describe observations of CPT induced by Raman pulses in cold atoms. While the three-level theory presented in Sec. II does not address the more complex excited-state hyperfine structure encountered with real atoms, our experiments exhibit clear signatures of population trapping and the results are in accord with central qualitative predictions of the theory. Our approach differed from previous work in that we produced and detected non-steady-state CPT effects using atom interferometry in a cold dilute vapor, rather than steady-state CPT induced and detected by pump-probe beams in a vapor cell (e.g., [11]). Our basic method was to prepare an ensemble of cold cesium atoms in the $|F = 3, m_F = 0\rangle$ ground state, apply long Raman pulses in free space, and observe the resultant population and coherences. As described below, care was taken to discriminate against the contribution of the initial polarizations. CPT-induced population differences and coherences were observed to be induced by both velocity-insensitive and velocity-sensitive Raman pulses. Use of velocity-insensitive Raman pulses afforded an expedient path to a first demonstration, because of the ease of implementation and the suppression of systematic effects due to atom cloud temperature and laboratory vibrations. However, inasmuch as velocity-insensitive Raman interferometers are used mostly as an experimental diagnostic, velocity-insensitive CPT effects are of limited practical interest. Velocity-sensitive Raman transitions serve as atom optics in high-precision atom interferometry experiments. Thus CPT effects induced by velocity-sensitive Raman pulses have implications for precision measurement results obtained with Raman pulse interferometry (e.g., [1,18]), which are discussed at the end of this section.

The experimental apparatus has been described in detail in [19], so we provide a brief summary here. Our experiments begin with an ensemble of cesium atoms loaded in a magneto-optic trap and cooled in far-detuned optical molasses to 5 μK. The atoms are then prepared in the magnetically insensitive $|F = 3, m_F = 0\rangle$ state by optical pumping, and other atoms are blown away by laser light resonant with the $F = 4 \rightarrow F' = 5$ cycling transition. We can also select a narrower velocity distribution ($<0.5\,\mu$K) with a velocity-sensitive Raman pulse. The Raman laser beams are generated by an 852-nm laser that is stabilized to a detuning of $\Delta = -1.25$ GHz from the frequency difference between ground-state $F = 4$ and excited-state $F' = 2$ hyperfine levels. Sidebands at the hyperfine splitting are created by phase modulation in an electro-optic modulator. The Raman beams are then collimated to a 1 cm ($1/e^2$) diameter and are retroreflected to drive velocity-sensitive Raman transitions. The atoms are interrogated in free fall by the vertically oriented Raman beams, with the Doppler shift lifting the degeneracy between transitions with opposite $\vec{k}_{\rm eff}$. The Raman detuning is chirped to compensate for the Doppler shift of the accelerating atoms [$\dot{\delta} = \vec{k}_{\rm eff} g/(2\pi) \approx 23$ kHz/ms]. Finally, the interferometer phase is extracted by measuring the populations in the $|F = 3, m_F = 0\rangle$ and $|F = 4, m_F = 0\rangle$ states with normalized laser-induced fluorescence.

A. Velocity-insensitive Raman pulses

We have characterized the dependence of CPT effects on Raman pulse duration, Raman detuning, Rabi frequency, and laser detuning. In addition to providing an expedient demonstration of CPT effects, these measurements also provided an upper bound on the effect that could be expected to be produced

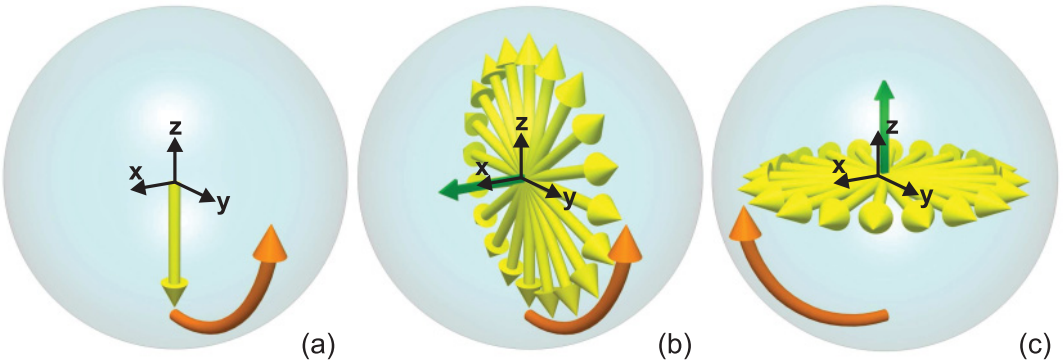

FIG. 2. (Color online) Bloch-sphere representation of a two-pulse experiment for detecting coherently trapped population induced by a velocity-insensitive Raman pulse. (a) The first Raman pulse rotates the initial polarization along $-\mathbf{z}$ about the $\mathbf{x}$ axis. (b) At long first-pulse durations, the initial polarization of the ensemble is dispersed in the $\mathbf{y}-\mathbf{z}$ plane by a spatially varying Rabi frequency. A polarization along the effective drive field (vector along $\mathbf{x}$) is induced by CPT. (c) After a brief dwell time, a $\pi/2$ pulse at a phase $\pm 90^\circ$ relative to the first pulse rotates the induced coherence onto $\mathbf{z}$, where it is measured as a population difference. The initial ensemble contributes no net polarization.

by velocity-sensitive Raman pulses. Velocity-sensitive Raman pulse CPT effects are described in the next section.

To distinguish coherently trapped population from population remaining in bright states, Raman pulses with duration greater than $10t_\pi$ were applied to dephase the ensemble with the spatial distribution of Rabi frequencies in the Raman beam. The resulting visibility of Rabi oscillations from the initial polarization was less than 1% (in other words, $\langle P_z \rangle = 0$ for the ensemble-averaged pseudospin and the average transition probability was 50%). When subjected immediately to population readout, the ensemble appeared completely dephased, i.e., the population trapped in a dark superposition had no P_z component. However, by subsequently applying a $\pi/2$ pulse, as depicted in Fig. 2, the coherence was rotated into an observable population difference. The $\pi/2$ pulse induced right-hand rotation of the induced coherence. An induced coherence parallel to the effective field $\vec{\Omega}$ of the first pulse would then produce maximum (minimum) population transfer at -90° ($+90^\circ$). Interferograms obtained by varying the $\pi/2$ pulse phase (Fig. 3) indicate that the induced coherence was parallel to the effective drive field for negative Δ and antiparallel for positive Δ, consistent with a CPT effect. Figure 3 is expressed in terms of transition probability with peak-to-peak variation of about 23%. On the Bloch sphere of Fig. 2, this corresponds to an induced polarization of magnitude 0.23 on a scale where all atoms exclusively in one ground state correspond to a polarization of magnitude unity.

Figure 4 depicts the measured dark-state population induced by resonant Raman pulses for a range of pulse durations. Recalling that our theory predicts a trapped population scaling with the pulse area, the pulse duration is scaled in units of t_π. Similar curves were obtained with Rabi frequencies over a range of 20–100 kHz, which is consistent with the theory. For pulse areas less than 40π, the trapped population increased linearly. Trapping appeared to saturate at $60-80t_\pi$, and thereafter, losses due to spontaneous emission and weak coupling out of the dark state dominated. A linear fit over the low-pulse area data estimates that a π pulse traps 1.5% of the population for $\Delta = -1.65$ GHz. Direct measurements of CPT for Raman pulses with pulse areas under 10π were not possible because of inadequate dephasing of the initial ensemble. Nevertheless, as Fig. 5 shows, the phase of the

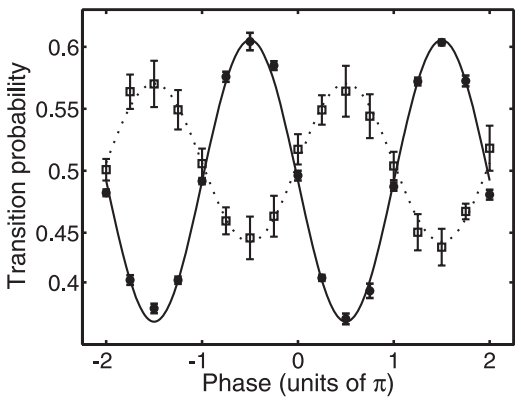

FIG. 3. Dark-state population observed with velocity-insensitive $75\pi - \pi/2$ interferometers at positive (filled circles: $\Delta = -1.25$ GHz; open squares: $\Delta = +2.5$ GHz). Both detunings are referenced to the $F = 4 \rightarrow F' = 2$ frequency. As predicted by the theory in Sec. II, CPT induces dark-state polarizations at opposite phases for positive/negative laser detunings.

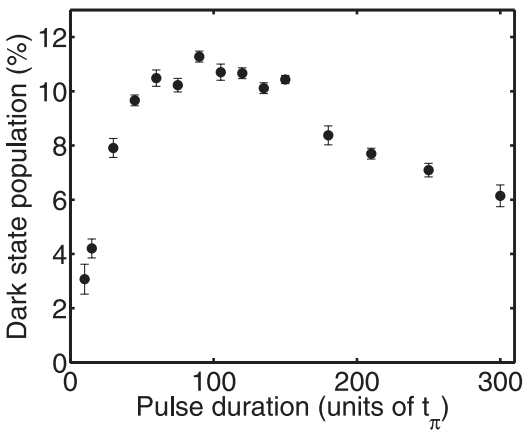

FIG. 4. Dark-state population induced by resonant, velocity-insensitive Raman pulses ($\Delta = -1.25$ GHz).

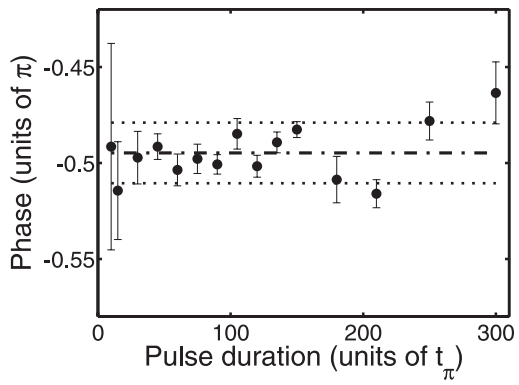

FIG. 5. Phase of dark-state coherences induced by velocity-insensitive Raman pulses. A phase of $-\pi/2$ corresponds to induced polarization parallel to the effective drive field $\vec{\Omega}$.

observed coherences at all longer pulse durations remained at the expected phase of $\Delta\phi = -\pi/2$, an important necessary condition for identification of the result as a CPT effect. Figure 6 shows trapped population versus pulse duration curves for several laser detunings, from -1.25 to -3 GHz. Maximum trapping was observed at $\Delta \approx -1.5$ GHz. The theory of Sec. II predicts a constant asymptotic dark-state polarization, independent of laser detuning. Figure 6 shows that induced polarizations over a factor-of-2 variation in laser detuning were similar, reflecting only weak dependence on laser detuning.

Lastly, we measured population differences induced by off-resonant Raman pulses, as predicted by the theory in Sec. II. We began with a sample of atoms prepared in the $|F = 3, m_F = 0\rangle$ state ($\vec{P} = -\hat{z}$) and formed a coherent superposition of the $|F = 3, m_F = 0\rangle$ and $|F = 4, m_F = 0\rangle$ levels with a Raman $\pi/2$ pulse. After a brief dwell time, an off-resonant Raman pulse dephased this initial coherence and induced a dark-state polarization. Since the laser frequency difference changed between the first and second pulse, the laser difference phase for the second pulse was shifted such that the initial polarization was dispersed with an average transition probability of 50% (i.e., $\langle P_z \rangle = 0$). We experimentally

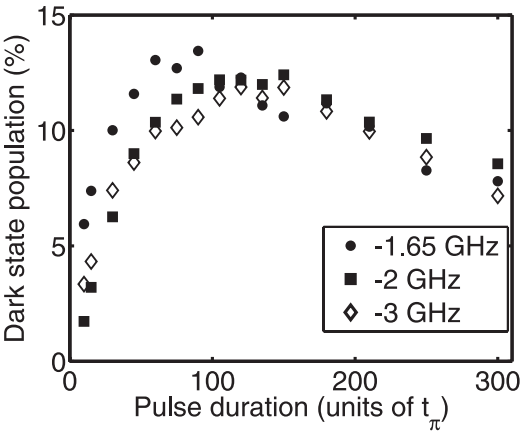

FIG. 6. Induced dark-state population obtained with several Raman laser detunings. The magnitude of trapped population is weakly dependent on Raman laser detuning.

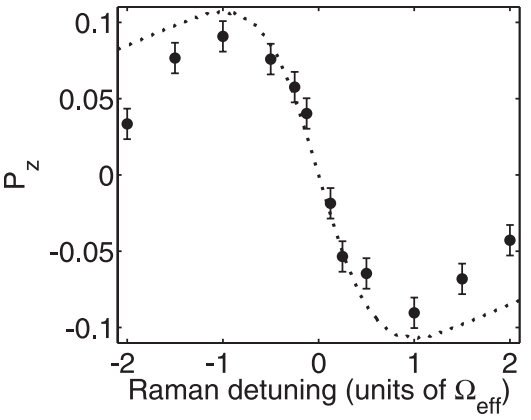

FIG. 7. Measurements P_z of dark-state population induced by off-resonant Raman pulses. The dashed curve represents a theoretical prediction based on an extension of the three-state theory permitting spontaneous decay out of the two coupled ground states.

determined this phase offset for each chosen Raman detuning using a $\pi/2 - \pi^*$ interferometer (π^* denotes an off-resonant π pulse) with the same dwell time between pulses. Finally, the P_z component of the trapped population was measured by reading out the population transfer and comparing to 50%. In order to suppress systematic errors resulting from drifting Raman beam power, we calibrated $P_z = 0$ in every other measurement by applying a single resonant 15.5π pulse and measuring population transfer.

Figure 7 shows the induced P_z for $\Delta = -1.25$ GHz and a second pulse duration of $40t_\pi$. In agreement with theory, the profile is antisymmetric about zero detuning and the overall sign of P_z is opposite that of the Raman detuning. We observed extrema at $\delta = \pm\Omega_{\text{eff}}$. For $\delta < |\Omega_{\text{eff}}|$, the observed P_z dependence resembles the z projection of a polarization vector aligned with the effective drive field and with a magnitude equal to the coherence induced by a resonant Raman pulse (0.19, or population ≈9.5%, for a 40π pulse). Figure 7 also depicts a theoretical prediction from a simple extension of the theory presented in Sec. II, which permits spontaneous emission to uncoupled ground states. We assumed a probability of spontaneous emission to uncoupled ($m_F \neq 0$) ground-state levels based on dipole matrix elements for cesium. At larger Raman detunings, observed CPT effects are smaller than predicted by the three-level theory; this discrepancy is expected since the theory does not account for multiple excited states. These measurements further support our theoretical prediction that coherent population trapping induces a polarization parallel to the effective drive field vector.

B. Velocity-sensitive Raman pulses

To detect CPT effects with velocity-sensitive Raman pulses, we used a slightly different method than that described above for velocity-insensitive Raman pulses. We first prepared atoms in the $|F = 3, m_F = 0\rangle$ level and then applied a microwave $\pi/2$ pulse. Since the wavelength of the microwave transition (∼3.3 cm) is large compared to the cloud size (∼1 mm), all of the atoms experience a similar phase. After a brief dwell time, a long, resonant velocity-sensitive Raman pulse dispersed the ensemble and induced CPT. The atoms experience a

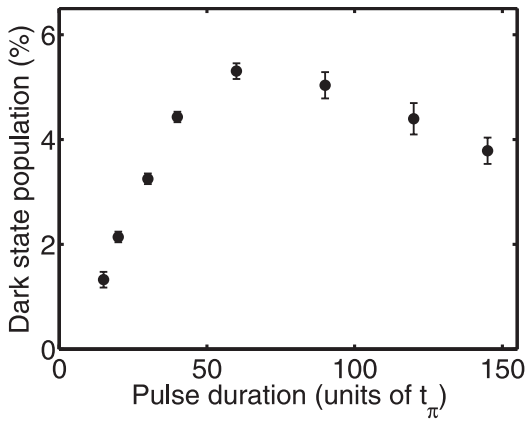

FIG. 8. Dark-state population induced by velocity-sensitive Raman pulses. These values have not been adjusted to compensate for the reduced contrast of the interferometer.

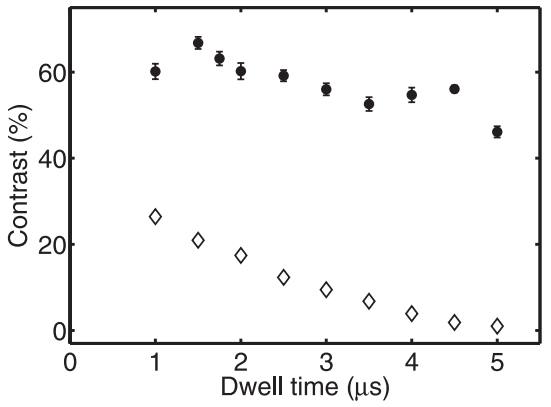

FIG. 9. Contrast achieved with a velocity-sensitive, nonoverlapping $\pi/2-\pi/2$ interferometer with (circles) and without (diamonds) velocity selection. The contrast of this nonoverlapping interferometer indicates the efficiency with which we can measure dark-state population induced by velocity-sensitive Raman pulses. Velocity selection clearly suppresses decoherence due to cloud diffusion.

distribution of Raman phases because of their initial spread in position over many effective wavelengths ($2\pi/|\vec{k}_{\rm eff}| \approx$ 426 nm), thoroughly scrambling the phase of the initial coherence with respect to the position-dependent Raman effective drive field $\vec{\Omega}$. After a very short dwell time (typically $1-2$ μs), a Raman $\pi/2$ pulse at variable phase projected the induced polarization onto the z axis.

Figure 8 shows the profile of dark-state population versus pulse duration for a laser detuning of $\Delta = -1.25$ GHz and a Rabi frequency of 80 kHz. This curve resembles the measurements of dark-state population for varying Raman pulse duration in the analogous velocity-insensitive experiment (compare with Fig. 4). Again, the effect appears to saturate between 60 and 80 t_π and decays at longer pulse durations. While the magnitude of the dark-state population appears smaller than what was measured with velocity-insensitive beams, these measurements underestimate the trapped population because the interferometer is only partially overlapping and consequently exhibits poorer phase contrast (our measure for the trapped population). To compensate for this inefficiency, we measured the contrast of a velocity-sensitive $\pi/2-\pi/2$ interferometer for a range of dwell times. Figure 9 shows that less than 30% contrast was observed for a 7-μK cloud. With velocity selection, however, interrogating atoms with a temperature of 400 nK produced greater than 55% contrast for the same dwell times (shown by the upper curve in Fig. 9). In both cases, adjusting the measured dark-state population by the two-pulse interferometer visibility leads to an estimated maximum induced dark-state coherence of magnitude of 0.18 (9% population), somewhat smaller than the maximum value observed with velocity-insensitive Raman pulses. We also expect less efficient population trapping by velocity-sensitive Raman pulses due to the Doppler broadening of the resonance. Based on the slope at short pulse durations, we estimate an induced dark-state coherence of magnitude 0.0074 (population of 0.37%) for a π pulse.

C. Impact of CPT on a $\pi/2-\pi-\pi/2$ interferometer

We now consider a simple estimate of the impact of an induced dark-state coherence on a velocity-sensitive $\pi/2-\pi-\pi/2$ interferometer, which is the most common sequence for acceleration and rotation rate measurements. The first Raman pulse induces a small coherence 90° out of phase with the primary coherence created by tipping the initial polarization into the $x-y$ plane. The induced coherence is orthogonal to the primary coherence, and effectively shifts the net phase by the ratio of the induced coherence magnitude to that of the primary coherence. The second pulse again transfers population to a dark state; however, each atom in the ensemble experiences a different effective drive field ($\vec{\Omega}$) phase because of the thermal velocity distribution. The ensemble average of the error phase induced by the second Raman pulse is then zero. The third pulse also induces a coherence, but for near-resonant Raman pulses it does not affect the final state population since the induced polarization is in the $x-y$ plane. Thus, we expect a phase shift due to the first Raman pulse, with a magnitude equal to the ratio of the induced coherence to the primary coherence. We have shown that the magnitude of CPT-induced polarization is roughly independent of Rabi frequency, so that we can use our measurements to estimate the induced phase in interferometers using cesium. We estimated that velocity-sensitive Raman pulses produce coherences of magnitude 0.0074 per π pulse. Correspondingly, we estimate that a $\pi/2-\pi-\pi/2$ interferometer should register a phase shift of $\Delta\phi \approx 0.0074/2 \approx 3.7$ mrad phase shift. In a previous high-precision cesium gravimeter [1,18], this phase shift corresponded to a gravity offset of $\approx$1 μGal. An error of this magnitude is four times smaller than the claimed experimental error, so a CPT-induced error of the estimated size would not significantly affect their results.

In presenting interferometer phase-shift estimates, we concede the preferability of directly measuring an interferometer phase shift induced by CPT. In principle, the phase shift could be measured by alternately running $(\pm\pi/2)-\pi-\pi/2$ interferometers and comparing their phases. A deviation of the relative phase from π would be ascribed to a CPT-induced shift. However, our apparatus presently lacks sufficient resolution to detect phase offsets of the estimated magnitude.

Finally, we note that a CPT-induced interferometer phase shift would be independent of the Raman beam wave vector

$\vec{k}_{\text{eff}}$. The method of propagation direction reversal should then suppress the resulting bias with averaged measurements (phase shifts resulting from ac Stark shifts are suppressed in a similar fashion), because the $\vec{k}_{\text{eff}}$-proportional contribution to the signal will reverse sign while the interferometer phase shift due to CPT will not.

IV. CONCLUSIONS

We have presented a simple density matrix theory which, by including spontaneous emission, predicts significant coherent population trapping in a three-level atom at large laser detunings typically used in Raman pulse interferometry. By performing adiabatic elimination on the excited state, we represented the reduced two-state system as a pseudospin precessing about an effective drive field on a Bloch sphere, with CPT acting to induce a polarization along the effective drive field. The assumed Λ configuration afforded a simple presentation but did not yield a theory with quantitative predictive capability. In future work, a numerical simulation incorporating multiple excited states could address the effect of multiple possible dark states, as well as address the potential for variation in the magnitude of these effects in other atomic species (e.g., rubidium).

The experiments described in Sec. III detected CPT in both velocity-insensitive and velocity-sensitive Raman pulse atom interferometry. We investigated the dependence of the induced dark-state population on Raman pulse duration, two-photon Rabi frequency, laser detuning, and Raman detuning. In the velocity-sensitive case, we showed that Raman pulses induced nearly as much dark-state population in colder ensembles ($<$500 nK) as that induced by velocity-insensitive pulses. Our experimental approach avails a method for producing and manipulating coherences and population differences arising from transient CPT in cold atoms. We are not aware of a previous demonstration of CPT-induced population difference.

Finally, we have argued that coherent population trapping should contribute to the phase of a Raman $\pi/2 - \pi - \pi/2$ interferometer as a systematic offset. This phase shift should be accounted for in high-precision interferometer measurements. Given the scale of the effect, and that the impact of dark-state coherences on interferometer phase is independent of the Raman beam wave vector, the method of propagation direction reversal [14] should suppress this bias with averaged measurements. While the impact of CPT has been discussed in the context of a three-pulse interferometer, other Raman interferometers should also experience phase shifts arising from this effect. A simple example is a velocity-insensitive Raman $\pi/2 - \pi/2$ clock measurement, in which the first pulse induces a dark-state coherence and offsets the phase read out by the second pulse. Moreover, the clock measurement is independent of $\vec{k}_{\text{eff}}$, thereby precluding the use of $\vec{k}_{\text{eff}}$-reversal suppression. Since the effect is only weakly dependent on Rabi frequency and laser detuning, a Raman beam with well-controlled parameters should produce a stable phase shift, so that the principal effect would likely pertain more to clock accuracy than stability.

ACKNOWLEDGMENT

D.B. and K.K. acknowledge support from the C.S Draper Laboratory Office of Education. This work was supported by the Charles Stark Draper Laboratory IR&D program.

[1] A. Peters, K. Chung, and S. Chu, Nature **400**, 849 (1999).
[2] T. Gustavson, A. Landragin, and M. Kasevich, Classical Quantum Gravity **17**, 2385 (2000).
[3] J. Fixler, G. Foster, J. McGuirk, and M. Kasevich, Science **315**, 74 (2007).
[4] H. Müller, S.-w. Chiow, S. Herrmann, and S. Chu, Phys. Rev. Lett. **102**, 240403 (2009).
[5] H. Müller, S.-w. Chiow, Q. Long, S. Herrmann, and S. Chu, Phys. Rev. Lett. **100**, 180405 (2008).
[6] P. Cladé, S. Guellati-Khélifa, F. Nez, and F. Biraben, Phys. Rev. Lett. **102**, 240402 (2009).
[7] A. Gauguet, T. E. Mehlstäubler, T. Lévèque, J. Le Gouët, W. Chaibi, B. Canuel, A. Clairon, F. P. Dos Santos, and A. Landragin, Phys. Rev. A **78**, 043615 (2008).
[8] B. Young, M. Kasevich, and S. Chu, in *Atom Interferometry*, edited by P. Berman (Academic Press, New York, 1997), pp. 363–406.
[9] G. Alzetta, A. Gozzini, L. Moi, and G. Orriols, Nuovo Cimento B **36**, 5 (1976).
[10] E. Arimondo and G. Orriols, Lett. Nuovo Cimento **17**, 333 (1976).
[11] H. Gray, R. Whitley, and J. C. R. Stroud, Opt. Lett. **3**, 218 (1978).
[12] J. Kitching, S. Knappe, M. Vukicevic, L. Hollberg, R. Wynands, and W. Weidmann, IEEE Trans. Instrum. Meas. **49**, 1313 (2000).
[13] M. O. Scully and M. Fleischhauer, Phys. Rev. Lett. **69**, 1360 (1992).
[14] D. S. Weiss, B. C. Young, and S. Chu, Appl. Phys. B **59**, 217 (1994).
[15] R. Stoner, D. Butts, J. Kinast, and B. Timmons, J. Opt. Soc. Am. B **28**, 2418 (2011).
[16] R. Loudon, *The Quantum Theory of Light* (Oxford Science Publications, New York, 1990).
[17] A. Peters, High Precision Gravity Measurements Using Atom Interferometry, Ph.D. thesis, Stanford University, 1998.
[18] H. Müller, A. Peters, and S. Chu, Nature **463**, 926 (2010).
[19] D. Butts, J. Kinast, B. Timmons, and R. Stoner, J. Opt. Soc. Am. B **28**, 416 (2011).